DOI: 10.1002/((please add manuscript number))
**Article type: Communication**

# Metal-Organic Frameworks Decorated Cuprous Oxide Nanowires for Long-lived Charges Applied in Photocatalytic $CO_2$ Reduction to $CH_4$

*Hao Wu, Xin Ying Kong, Xiaoming Wen, Siang-Piao Chai, Emma C. Lovell, Junwang Tang, Yun Hau Ng**

H. Wu, Prof. Y.H. Ng
School of Energy and Environment
City University of Hong Kong
Tat Chee Avenue, Kowloon, Hong Kong, China
E-mail: yunhau.ng@cityu.edu.hk

H. Wu, Emma C. Lovell, Prof. Y. H. Ng
Particles and Catalysis Research Group
School of Chemical Engineering
The University of New South Wales
Sydney, NSW 2052, Australia

X. Y. Kong, Prof. S-P. Chai
Multidisciplinary Platform of Advanced Engineering
Chemical Engineering Discipline, School of Engineering
Monash University
Jalan Lagoon Selatan, Bandar Sunway, 47500 Selangor, Malaysia

X. Wen
Centre for Translational Atomaterials
Faculty of Science Engineering and Technology
Swinburne University of Technology
John Street, Hawthorn, VIC 3122, Australia

Prof. J. Tang
Department of Chemical Engineering
University College London
Torrington Place, London WC1E 7JE (UK)

**Abstract:** Improving the stability of cuprous oxide ($Cu_2O$) is imperative to its practical applications in artificial photosynthesis. In this work, $Cu_2O$ nanowires are encapsulated by metal-organic frameworks (MOFs) of $Cu_3(BTC)_2$ (BTC = 1,3,5-benzene tricarboxylate) using a surfactant-free method. Such MOFs not only suppresses the water vapor-induced corrosion of $Cu_2O$, but also facilitate charge separation and CO2 uptake, thus resulting into a nanocomposite representing times improved activity and stability for selective photocatalytic carbon dioxide ($CO_2$) reduction into methane ($CH_4$) under mild reaction conditions. Furthermore direct transfer of photogenerated electrons from the conduction band of $Cu_2O$ to the LUMO level of non-excited $Cu_3(BTC)_2$ has been evidenced by time-resolved photoluminescence. This work proposes effective strategy for CO2 conversion by a synergy of charge separation and CO2 adsorption, lending to enhanced photocatalytic reaction when MOFs are integrated with metal oxide photocatalyst.

Mimicking the natural photosynthesis for capturing the gaseous $CO_2$ emissions and converting them into high-value-added chemicals is a potential capstone technology. The outstanding challenges remain in the design of efficient photocatalyst systems featuring (i) $CO_2$ capture on catalytic sites, (ii) photon-to-electron generation, (iii) charge separation and (iv) long-term stability.[1–4]

Concerning photon-harvesting ability, $Cu_2O$ is ordinarily endowed with efficient visible-light absorption and a conduction band position favorable for $CO_2$ reduction.[5–7] However, its practical application is bounded by insufficient stability.[8,9] To overcome this hindrance, we rationally encapsulated one-dimensional (1-D) $Cu_2O$ nanowires in the Cu based MOFs of $Cu_3(BTC)_2$. The strategy is built by the following reasons: 1) Cu-based MOFs as the protecting shell of the composite can protect unstable semiconductors inside from the water-vapor induced corrosion. 2) Integrating $Cu_2O$ is capable of improving the visible-light absorption of MOFs (avoid using noble-metal photosensitiser); while MOFs with unsaturated coordinated single Cu sites can be the active components that reduce the energy barrier for $CO_2$ reduction and stabilize the reaction intermediates.[10–16] 3) 1-D nanostructure contributes to a high surface-to-volume ratio, short lateral charge transport length, and low light-reflectivity, which usually demonstrates higher photocatalytic efficiencies.[17–20] 4) The framework of $Cu_3(BTC)_2$ with good $CO_2$ absorption capacity can provide a dense $CO_2$ atmosphere for the reduction reactions.

Although $Cu_2O$ possesses the appropriate band edge positions to realize CO and $CH_4$ production under visible-light irradiation,[21] the $CH_4$ formation requires eight electrons which is more challenging than the CO production from a kinetic point of view.[22] In this work, we describe a gaseous photocatalytic system with water vapor as the electron donor for selective $CO_2$ reduction to $CH_4$ using the composite of $Cu_2O@Cu_3(BTC)_2$ grown on copper mesh (CM). The transformed $Cu_3(BTC)_2$ shell of the composite photocatalyst sheet of $Cu_2O@Cu_3(BTC)_2$/CM shows a good affinity with the underlying $Cu_2O$ and provides considerable surface areas for the $CO_2$ adsorption and reduction. Intriguingly, time-resolved photoluminescence (TRPL) measurements reveal the direct transfer of photogenerated electrons from the conduction band of $Cu_2O$ nanowires to the non-excited $Cu_3(BTC)_2$ (LUMO level), inducing a long-lived

charge separated state following bandgap excitation. The resulting $Cu_2O@Cu_3(BTC)_2$/CM composite achieves a selective reduction of $CO_2$ to $CH_4$ with significantly improved stability and an over 2-fold increase of yield compared to the bare $Cu_2O$/CM sample, under visible-light irradiation.

The $Cu_2O@Cu_3(BTC)_2$ core-shell nanowires were fabricated on porous CM, from its $Cu_2O$ nanowires/CM precursor (details in the Experimental Section). Considering the relatively slow dissolving rate of $Cu^{2+}$ from $Cu_2O$ and the fast reaction kinetics of nucleation for $Cu_3(BTC)_2$, the $Cu_2O$ nanowires were enwrapped by the framework of $Cu_3(BTC)_2$ (Scheme 1). The color of CM changed from reddish-brown to red and then green as shown in Figure 1a, suggesting the growth of $Cu_2O$ and $Cu_3(BTC)_2$ on CM, respectively. Furthermore, Figure 1b-d show the top-view scanning electron microscope (SEM) images of CM, $Cu_2O$/CM, and $Cu_2O@Cu_3(BTC)_2$/CM samples, respectively, demonstrating the change of morphologies from the flat substrate to the nanowire structures. Both $Cu_2O$ and $Cu_2O@Cu_3(BTC)_2$ nanowires have an average length longer than 8 μm. A more detailed investigation was conducted by transmission electron microscopy (TEM). As shown in Figure 1e and 1f, the $Cu_2O$ inner core with a diameter of ~400 nm and MOF outer shell with a thickness of ~300 nm were identified. The corresponding energy dispersive X-ray (EDX) line scan (Figure 1g) and mapping images (Figure 1h and 1i) further show that the solid $Cu_2O$ has a higher intensity of Cu than the porous $Cu_3(BTC)_2$. The $Cu_2O@Cu_3(BTC)_2$ presents relatively higher intensities of Cu and O in the middle with an intensity of carbon (C) homogenously distributed over the outer layer, thus suggesting its core-shell structure.

The crystalline phases were confirmed by X-ray diffraction (XRD) shown in Figure 1j. Both $Cu_2O$/CM and $Cu_2O@Cu_3(BTC)_2$/CM samples presented diffraction peaks indexed to $Cu_2O$ and Cu (JCPDS 080-7711). After the growth of $Cu_3(BTC)_2$, the peaks of $Cu_3(BTC)_2$ • hydrate in the range of 5-30° were appeared (JCPDS 064-0936). The hydrate in the structure is attributed to the coordinated water molecules in $Cu_3(BTC)_2$.[23,24] As further determined by the Rietveld refinement, the weights of $Cu_2O$ in $Cu_2O$/CM and $Cu_2O@Cu_3(BTC)_2$/CM samples are ~12.5 mg and ~8.7 mg, respectively. The UV-vis diffuse reflectance spectrum implies that the coating of $Cu_3(BTC)_2$ does not alter the band structure of $Cu_2O$ for

harvesting visible-light (Figure S1). The slightly decreased light absorbance for $Cu_2O@Cu_3(BTC)_2$/CM sample is possibly caused by the partial transformation of $Cu_2O$ during the topotactic synthesis.

The photocatalytic performance for gaseous $CO_2$ reduction was carried out in a continuous gas flow reaction system using water vapor as the electron donor (details in the Experimental Section). The main product is $CH_4$ for the prepared samples. Neither CO, $C_2$-$C_4$ nor $H_2$ were detected for all the tested systems (Figure S2a-c). In addition, control experiments were conducted under identical conditions (details in the Experimental Section). Negligible products of $CO_2$ reduction were observed in the controlled situations, which suggest that those parameters including visible light, $CO_2$, water vapor and photocatalyst are prerequisites for the photocatalytic gaseous $CO_2$ reduction to take place (Figure S2d). Also, the likelihood of photolysis from $Cu_3(BTC)_2$ could be excluded. In addition, the $^{13}C$ isotope experiment reveals that $CH_4$ originates from the $CO_2$ reduction (Figure S3).

Figure 2a shows the time-dependent conversion yields of $CO_2$ into $CH_4$ using $Cu_2O$/CM and $Cu_2O@Cu_3(BTC)_2$/CM samples under visible-light irradiation. The $Cu_2O@Cu_3(BTC)_2$/CM sample attained a $CH_4$ yield of ~14.6 μmol $g^{-1}$ for 8 hours, which is more than two times higher than that of $Cu_2O$/CM (~6.3 μmol $g^{-1}$). The amount of oxygen generated with $Cu_2O@Cu_3(BTC)_2$/CM sample is close to two times of generated $CH_4$ (Figure S4), demonstrating that the electron source for the photocatalytic $CO_2$ reduction comes from the water oxidation. The solar-to-methane energy conversion efficiency (STM) of $Cu_2O@Cu_3(BTC)_2$/CM sample was determined to be 0.019% (detail in the Experimental Section). While the STM of $Cu_2O$/CM was only 0.010%. After reserving the samples for sixty-days in the atmospheric environment, the reusability of the prepared samples was investigated in other two-cycles under identical conditions. As shown in Figure 2a, the $Cu_2O@Cu_3(BTC)_2$/CM exhibited a fairly reproducible photocatalytic activity for all three cycles; while the drastically decreased performance of the bare $Cu_2O$/CM sample was observed. The accumulated gaseous photocatalytic activities for the $Cu_2O@Cu_3(BTC)_2$/CM and the $Cu_2O$/CM samples were presented in Table S1 and were normalized shown in Figure 2b. In contrast to the $Cu_2O$/CM sample, which lost more than 75% of its intrinsic activity,

the $Cu_2O@Cu_3(BTC)_2$/CM sample retained 81.3% of the original efficiency for the $CH_4$ production after three runs. XRD and Fourier transform infrared spectroscopy (FTIR) measurements were performed for the $Cu_2O@Cu_3(BTC)_2$/CM sample after the $CO_2$ reduction, which shows negligible change, thus indicating the crystal structure and the framework of $Cu_2O@Cu_3(BTC)_2$/CM retaining intact during the reactions (Figure S5a and S5b). While the bare $Cu_2O$/CM sample becomes amorphous, suggesting it is corroded after the reaction (Figure S5c). The improved stability induced by the $Cu_3(BTC)_2$ framework may be ascribed to the selective water vapor adsorption in the pore of $Cu_3(BTC)_2$, which avoids its direct contact to the exposed $Cu_2O$ surface.[9,10]

$N_2$ adsorption-desorption isotherms and $CO_2$ uptakes were firstly studied for the $Cu_2O$/CM and $Cu_2O@Cu_3(BTC)_2$/CM samples. The $Cu_2O@Cu_3(BTC)_2$/CM composite attained a Langmuir surface area of 13.2 $m^2 g^{-1}$, while the value of the bare $Cu_2O$/CM sample based on the total weight is less than 1 $m^2 g^{-1}$. More importantly, the maximum $CO_2$ uptake at room temperature based on the total weight for $Cu_2O@Cu_3(BTC)_2$/CM (2.0 $cm^3 g^{-1}$) is almost sevenfold over that of the bare $Cu_2O$/CM (0.3 $cm^3 g^{-1}$) sample (Figure 3a). The superiority of $Cu_2O@Cu_3(BTC)_2$/CM in $CO_2$ uptake is contributed by the porous composite structure with $Cu_2O$ encapsulated inside the $Cu_3(BTC)_2$ framework rather than being assembled on the surface.

To deeply understand the origin of the enhanced performance induced by encapsulating $Cu_2O$ into the framework of $Cu_3(BTC)_2$, we inspected the charge movement by recording photoluminescence (PL) spectra of the $Cu_2O$/CM and $Cu_2O@Cu_3(BTC)_2$/CM thin films. Compared to the bare $Cu_2O$ sample, the PL spectrum shows a decreased peak intensity at 500 nm and a new peak created between 600-700 nm for the $Cu_2O@Cu_3(BTC)_2$ composite (Figure 3b). The $Cu_3(BTC)_2$ has been reported to be a wide-bandgap semiconductor with the lowest unoccupied molecular orbital (LUMO) position of -3.7 eV vacuum energy level, which is slightly lower than the conduction band energy position of $Cu_2O$ (-3.2 eV).[17,21,25] The well-aligned energy levels are likely to facilitate the electron transfer from the conduction band of $Cu_2O$ to the LUMO level of $Cu_3(BTC)_2$, thus quenching the bandgap luminescence of $Cu_2O$. As shown in Figure

S6, the increased electrochemical active surface area (ECSA) of $Cu_2O@Cu_3(BTC)_2$/CM, compared to the bare $Cu_2O$/CM, also suggests that the induced electrons transport between $Cu_2O$ and $Cu_3(BTC)_2$ is permissible. When no $CO_2$ molecules exist in the testing environment, the energetic electrons stayed on the LUMO level of $Cu_3(BTC)_2$ are favorably recombined with the holes left on the valence band of $Cu_2O$,[26] thus generating a new PL peak following bandgap excitation (inset of Figure 3a). The energy difference of 0.5 eV between the conduction band of $Cu_2O$ and LUMO of $Cu_3(BTC)_2$ is well consistent with the PL peak difference (500 nm to 630 nm for 0.51 eV), which strongly suggest such an electron transfer and recombination. It is may arguable that the decreased PL peak is caused by the decreased light absorption upon the decoration of $Cu_3(BTC)_2$. Further insights into the dynamic charge transfer were revealed by TRPL (Figure 3c). The PL decay curves were fitted with a bi-exponential function (details in the Experimental Section) and compared at 500 nm and 630 nm emissions. The $Cu_2O$ sample shows a calculated average lifetime of 0.28 ns at 500 nm emission, while no signal was detected at 630 nm emission. Intriguingly, the average lifetime of $Cu_2O@Cu_3(BTC)_2$ at 630 nm (2.47 ns) is significantly longer than that at 500 nm emission (0.27 ns) and $Cu_2O$ (0.28 ns). The evidently longer lifetime indicates the significantly longer lifetime for the excited electrons attained by $Cu_2O@Cu_3(BTC)_2$ due to a slow recombination process between LUMO and valance band in $Cu_2O@Cu_3(BTC)_2$, which could be ascribed to the weakened interaction strength, overlap of the wavefunctions between the holes residing in $Cu_2O$ and the electrons in surface-bound $Cu_3(BTC)_2$, in agreement with the steady-state PL results. Although such interaction of charge carriers residing between semiconductor/semiconductor,[27] semiconductor/metal,[28] or semiconductor/metal-complex[29] have been reported in the literature, direct transfer of photogenerated electrons from the conduction band of semiconductor to the non-excited MOFs (LUMO level) is reported for the first time. Such charge transfer is benefited from the well-aligned energy levels as well as the good affinity between $Cu_2O$ and $Cu_3(BTC)_2$. The long-lived electrons localized in the $Cu_2O@Cu_3(BTC)_2$ hybrid nanostructure could be beneficial for the $CO_2$ reduction reactions.

In summary, $Cu_2O@Cu_3(BTC)_2$ composite photocatalysts have been synthesized by a surfactant-free method. Encapsulating $Cu_2O$ nanowires into the framework of $Cu_3(BTC)_2$ showed an enhanced gaseous

photocatalytic activity and stability for the selective $CO_2$ reduction to $CH_4$. Enlarged surface area and higher $CO_2$ uptakes were introduced by $Cu_3(BTC)_2$, which offered a dense $CO_2$ atmosphere for the reactions. Steady-steady and time-resolved PL collectively revealed that $Cu_3(BTC)_3$ being actively involved enables effective charge separation in $Cu_2O$. This study extends the understanding of the relationships between MOFs and metal oxides beyond their conventional physisorption/chemisorption type of interactions to now include charge separation (when energy levels are well aligned). These findings will stimulate future endeavour to develop highly efficient organic-inorganic hybrid photocatalysts.

**Supporting Information**
Supporting Information is available from the Wiley Online Library or from the author.

**Acknowledgments**

This project was financially supported by the Australian Research Council Discovery Project (DP180102540). The authors appreciate the facilities and technical support provided by the UNSW Mark Wainwright Analytical Centre.

Received: ((will be filled in by the editorial staff))
Revised: ((will be filled in by the editorial staff))
Published online: ((will be filled in by the editorial staff))

**Keyword:** carbon dioxide fixation, charge transfer, metal-organic frameworks, nanostructures, photosynthesis

References


[1] J. L. White, M. F. Baruch, J. E. Pander, Y. Hu, I. C. Fortmeyer, J. E. Park, T. Zhang, K. Liao, J. Gu, Y. Yan, et al., *Chemical Reviews* **2015**, *115*, 12888–12935.

[2] Y.-F. Song, L. Tan, S.-M. Xu, Z. Wang, Y. Xu, X. Wang, X. Hao, S. Bai, C. Ning, Y. Wang, et al., *Angewandte Chemie International Edition* **2019**, *58*, 1860–11867.

[3] N. Li, J.-J. Liu, Z.-F. Xin, Y.-L. Teng, Y.-Q. Lan, L.-Z. Dong, J. Liu, *Angewandte Chemie International Edition* **2019**, 5226–5231.

[4] S. Wang, M. Xu, T. Peng, C. Zhang, T. Li, I. Hussain, J. Wang, B. Tan, *Nature Communications* **2019**, *10*, 676.

[5] P. Wang, H. Wu, Y. Tang, R. Amal, Y. H. Ng, *The Journal of Physical Chemistry C* **2015**, *119*, 26275–26282.

[6] X. Chang, T. Wang, P. Zhang, Y. Wei, J. Zhao, J. Gong, *Angewandte Chemie International Edition* **2016**, *55*, 8840–8845.

[7] Y. A. Wu, I. McNulty, C. Liu, K. C. Lau, Q. Liu, A. P. Paulikas, C. J. Sun, Z. Cai, J. R. Guest, Y. Ren, et al., *Nature Energy* **2019**, *4*, 957–968.

[8] C. Y. Toe, Z. Zheng, H. Wu, J. Scott, R. Amal, Y. H. Ng, *Angewandte Chemie International Edition* **2018**, *57*, 13613–13617.

[9] H. Wu, Z. Zheng, C. Y. Toe, X. Wen, J. N. Hart, R. Amal, Y. H. Ng, *Journal of Materials Chemistry A* **2020**, *8*, 5638–5646.

[10] A. L. Wu, Y. Mu, X. Guo, W. Zhang, *Angewandte Chemie International Edition* **2019**, *58*, 9491–9495.

[11] M. ElCheikh Mahmoud, H. Audi, A. Assoud, T. H. Ghaddar, M. Hmadeh, *Journal of the American Chemical Society* **2019**, *141*, 7115–7121.

[12] A. M. Abdel-Mageed, B. Rungtaweevoranit, M. Parlinska-Wojtan, X. Pei, O. M. Yaghi, R. J. Behm, *Journal of the American Chemical Society* **2019**, *141*, 5201–5210.

[13] L. Shi, T. Wang, H. Zhang, K. Chang, J. Ye, *Advanced Functional Materials* **2015**, *25*, 5360–5367.

[14] H. X. Zhang, Q. L. Hong, J. Li, F. Wang, X. Huang, S. Chen, W. Tu, D. Yu, R. Xu, T. Zhou, et al., *Angewandte Chemie International Edition* **2019**, *58*, 1752–11756.

[15] J. Jiao, R. Lin, S. Liu, W.-C. Cheong, C. Zhang, Z. Chen, Y. Pan, J. Tang, K. Wu, S.-F. Hung, et al., *Nature Chemistry* **2019**, *11*, 222–228.

[16] R. Li, J. Hu, M. Deng, H. Wang, X. Wang, Y. Hu, H. L. Jiang, J. Jiang, Q. Zhang, Y. Xie, et al., *Advanced Materials* **2014**, *26*, 4783–4788.

[17] C.-Y. Lin, Y.-H. Lai, D. Mersch, E. Reisner, *Chemical Science* **2012**, *3*, 3482.

[18] Z. Zhang, R. Dua, L. Zhang, H. Zhu, H. Zhang, P. Wang, *ACS Nano* **2013**, *7*, 1709–1717.

[19] J. Luo, L. Steier, M. K. Son, M. Schreier, M. T. Mayer, M. Grätzel, *Nano Letters* **2016**, *16*, 1848–1857.

[20] H. Wu, H. L. Tan, C. Y. Toe, J. Scott, L. Wang, R. Amal, Y. H. Ng, *Advanced Materials* **2019**, 1904717.

[21] X. Deng, R. LI, S. Wu, L. Wang, J. Hu, J. Ma, W. Jiang, N. Zhang, X. Zheng, C. Gao, et al., *Journal of the American Chemical Society* **2019**, *141*, 10924–10929.

[22] X. Li, Y. Sun, J. Xu, Y. Shao, J. Wu, X. Xu, Y. Pan, H. Ju, J. Zhu, Y. Xie, *Nature Energy* **2019**, *4*, 690–699.

[23] L. Alaerts, E. Séguin, H. Poelman, F. Thibault-Starzyk, P. A. Jacobs, D. E. De Vos, *Chemistry - A European Journal* **2006**, *12*, 7353–7363.

[24] L. Jiao, Y. Wang, H. L. Jiang, Q. Xu, *Advanced Materials* **2017**, *1703663*, 1–23.

[25] K. T. Butler, C. H. Hendon, A. Walsh, *Journal of the American Chemical Society* **2014**, *136*, 2703–2706.

[26] S. M. Kobosko, J. T. Dubose, P. V Kamat, *ACS Energy Letters* **2019**, *5*, 221–223.

[27] J. Low, B. Dai, T. Tong, C. Jiang, J. Yu, *Advanced Materials* **2019**, *31*, 1802981.

[28] R. Jiang, B. Li, C. Fang, J. Wang, *Advanced Materials* **2014**, *26*, 5274–5309.

[29] A. Nakada, R. Kuriki, K. Sekizawa, S. Nishioka, J. J. M. Vequizo, T. Uchiyama, N. Kawakami, D. Lu, A. Yamakata, Y. Uchimoto, et al., *ACS Catalysis* **2018**, *8*, 9744–9754.

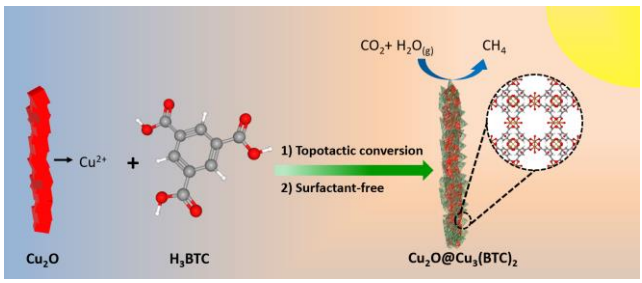


**Scheme 1.** Illustration of the synthetic route towards $Cu_2O@Cu_3(BTC)_2$ core-shell nanowires through a surfactant-free topotactic conversion strategy for selective gaseous photocatalytic carbon dioxide reduction to methane.

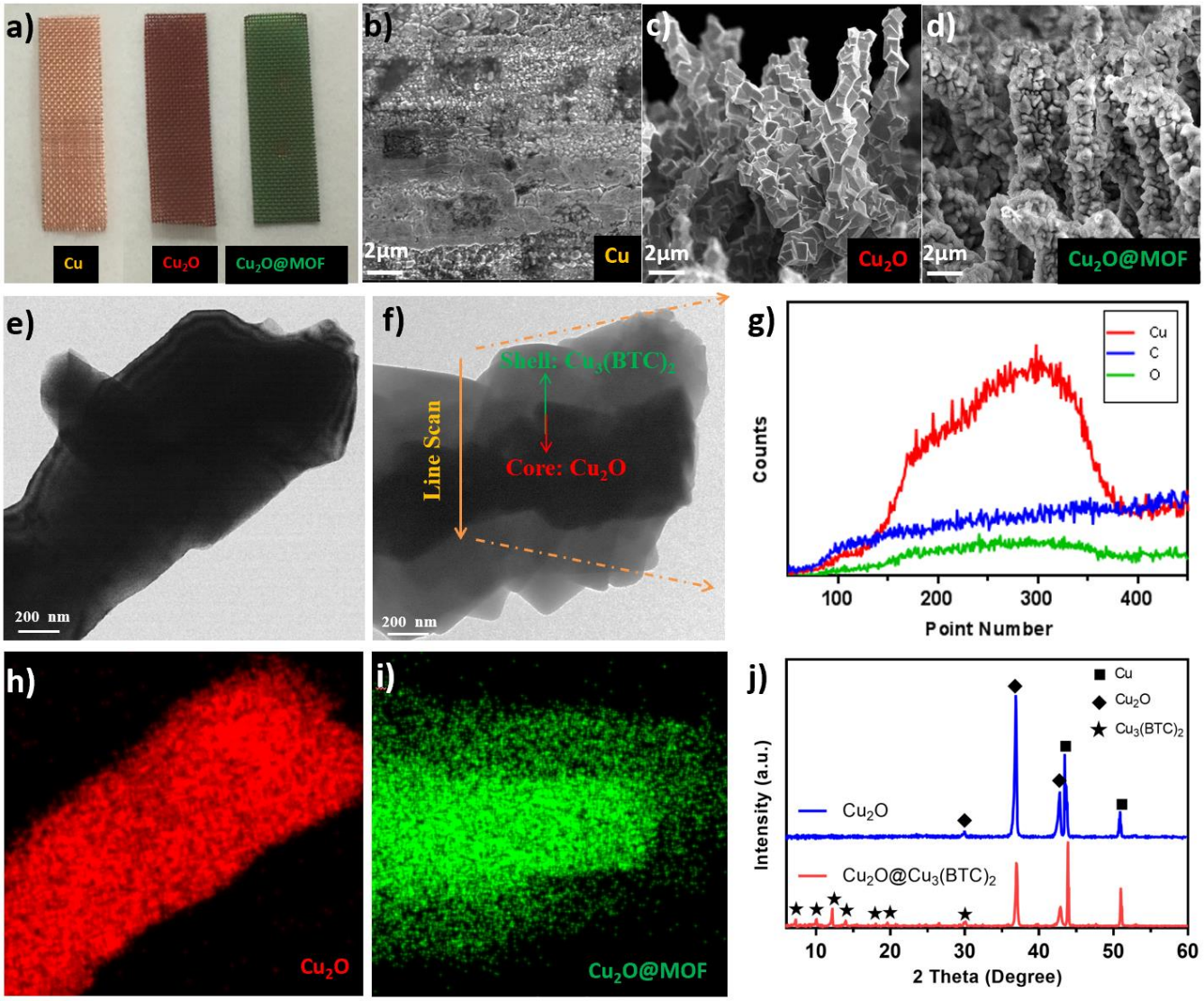


**Figure 1.** a) Real sample images and SEM images of Cu meshes in the synthesis process, from left to right: b) original Cu mesh, c) $Cu_2O$ nanowires, and d) $Cu_2O@Cu_3(BTC)_2$ hybrid nanoarrays. TEM images of e) $Cu_2O$, f) $Cu_2O@Cu_3(BTC)_2$, and g) the corresponding line scan of $Cu_2O@Cu_3(BTC)_2$. EDX mapping of the Cu element for h) $Cu_2O$ and i) $Cu_2O@Cu_3(BTC)_2$. j) XRD pattern of $Cu_2O$/CM and $Cu_2O@Cu_3(BTC)_2$/CM. *MOF shown in the figures stands for the $Cu_3(BTC)_2$ framework.

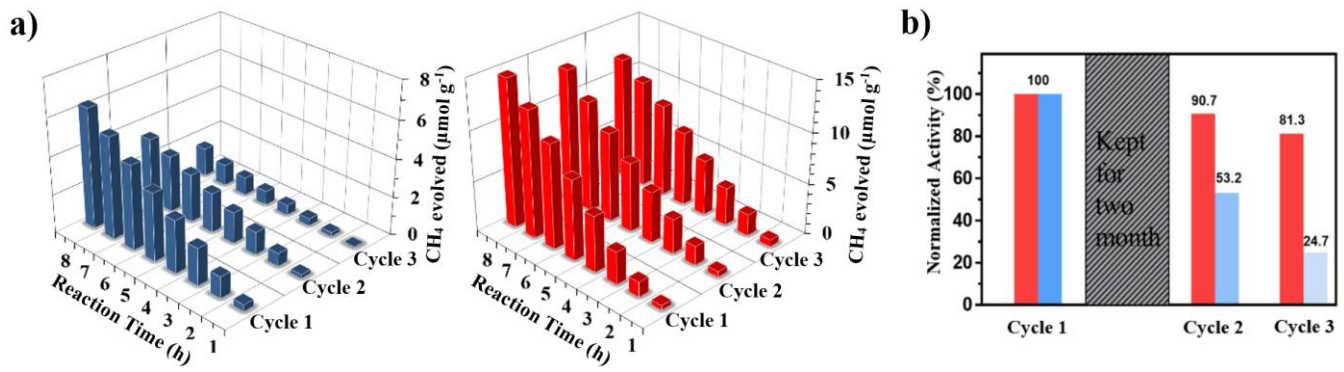


**Figure 2.** Photodurability tests for the $Cu_2O$/CM (blue) and $Cu_2O@Cu_3(BTC)_2$/CM (red) samples for recycling $CO_2$ photocatalytic reduction under visible-light irradiation (λ>400nm): a) Time course of the photocatalytic $CH_4$ production and b) normalized activity (%) of the $CH_4$ production for each cycle. No CO or alcohol products were found for any samples.

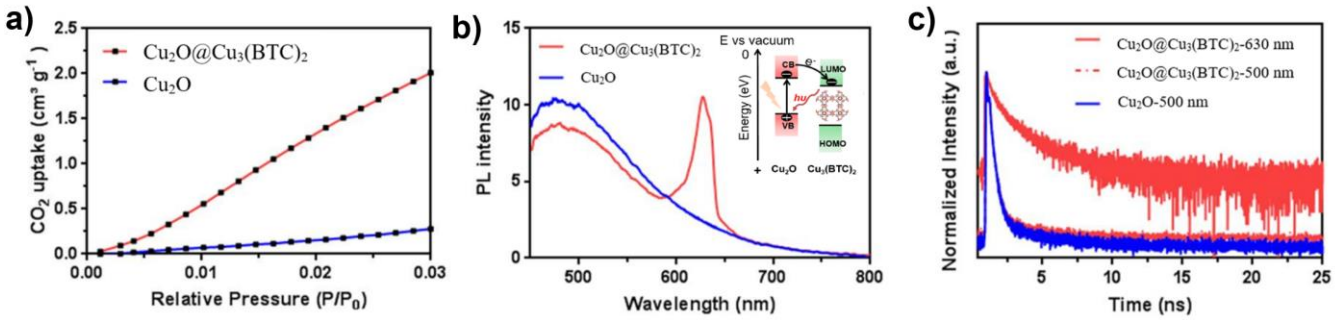


**Figure 3.** a) $CO_2$ adsorption behaviors of $Cu_2O$/CM and $Cu_2O@Cu_3(BTC)_2$/CM samples. The curves are plotted based on the total weights of materials. b) Steady-state photoluminescence (PL) and c) time-resolved PL of $Cu_2O$/CM and $Cu_2O@Cu_3(BTC)_2$/CM. The signals of time-resolved PL are monitored and compared at 500 nm and 630 nm separately. Inset: schematic illustration of corresponding energy band positions for photoexcited electron transfer in the $Cu_2O@Cu_3(BTC)_2$ core-shell nanostructures. CB-conduction band, VB-valence band, LUMO-lowest unoccupied molecular orbital, and HOMO-highest occupied molecular orbital.

**Entry for the Table of Contents**

## COMMUNICATION

**$Cu_2O$** nanowires are decorated with $Cu_3(BTC)_2$ by a surfactant-free method. The $Cu_2O@Cu_3(BTC)_2$ core-shell structure offers enlarged active surfaces and prolonged lifetime of separated electrons for $CO_2$ reduction into $CH_4$, exhibiting enhanced gaseous photocatalytic activity and stability compared to the bare $Cu_2O$.

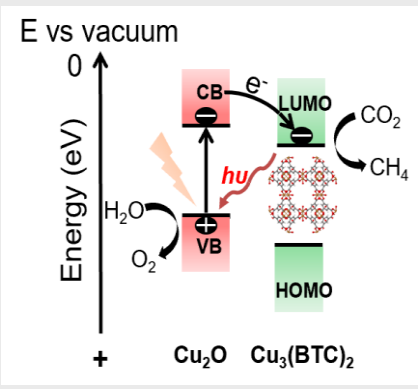


*Hao Wu, Xin Ying Kong, Xiaoming Wen, Siang-Piao Chai, Emma C. Lovell, Junwang Tang, Yun Hau Ng**

***Page No. – Page No.***

**Metal-Organic Frameworks Decorated Cuprous Oxide Nanowires for Long-lived Charges Applied in Photocatalytic $CO_2$ Reduction to $CH_4$**